ACS APPLIED MATERIALS & INTERFACES

Research Article

www.acsami.org

Synergistic Effect of Superhydrophobicity and Oxidized Layers on Corrosion Resistance of Aluminum Alloy Surface Textured by Nanosecond Laser Treatment

Ludmila B. Boinovich,* Alexandre M. Emelyanenko, Alexander D. Modestov, Alexandr G. Domantovsky, and Kirill A. Emelyanenko

A. N. Frumkin Institute of Physical Chemistry and Electrochemistry, Leninsky Prospect 31 Building 4, 119071 Moscow, Russia

Supporting Information

ABSTRACT: We report a new efficient method for fabricating a superhydrophobic oxidized surface of aluminum alloys with enhanced resistance to pitting corrosion in sodium chloride solutions. The developed coatings are considered very prospective materials for the automotive industry, shipbuilding, aviation, construction, and medicine. The method is based on nanosecond laser treatment of the surface followed by chemisorption of a hydrophobic agent to achieve the superhydrophobic state of the alloy surface. We have shown that the surface texturing used to fabricate multimodal roughness of the surface may be simultaneously used for modifying the physicochemical properties of the thick surface layer of the substrate itself. Electrochemical and wetting experiments demonstrated that the superhydrophobic state of the metal surface inhibits corrosion processes in chloride solutions for a few days. However, during long-term contact of a superhydrophobic coating with a solution, the wetted area of the coating is subjected to corrosion processes due to the formation of defects. In contrast, the combination of an oxide layer with good barrier properties and the superhydrophobic state of the coating provides remarkable corrosion resistance. The mechanisms for enhancing corrosion protective properties are discussed.

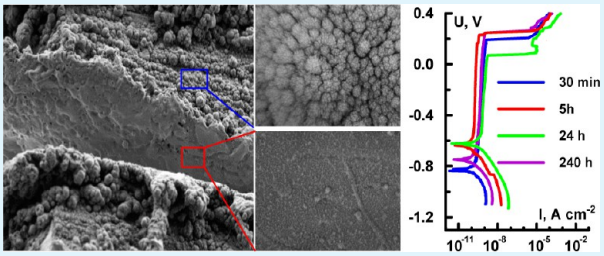

KEYWORDS: *anticorrosion coating, laser treatment, surface modification, superhydrophobicity, wetting, electrochemical methods*

INTRODUCTION

Aluminum and its alloys are commonly used in many fields of application. Among the large variety of aluminum alloys, aluminum−magnesium alloys are considered very prospective materials for the automotive industry, shipbuilding, aviation and space technology, construction, and medicine. The variety of applications of Al−Mg alloys in some cases requires versatile functional properties of the materials made from these alloys. In particular, the simultaneous provision of high corrosion resistance, electrical insulation and antifouling properties, and improved wear resistance, together with water-repellent surface properties of the material, is required. Despite good corrosion resistance in many environments, the use of Al−Mg alloys in mineralized chloride aqueous solutions or when the alloys contain intermetallic particles often results in pitting corrosion.[1,2] Thus, for industrial applications, it is highly desirable to develop coatings for materials made from Al−Mg alloys that increase protection against pitting corrosion and simultaneously provide the above-mentioned diversity of the surface functional properties. Over the years, a huge number of papers have been published on the treatment of aluminum alloy materials to enhance their corrosion resistance.[3−15]

A surface treatment that leads to achievement of the superhydrophobic state of metallic surfaces is an emerging technology that addresses many classic shortcomings of more traditional processes, such as sol−gel coating deposition, chemisorption of organic and inorganic inhibitors, deposition of barrier coatings, etc. Although the corrosion protection provided by superhydrophobic coatings on different metals shows stability in many practical cases,[12,15−18] some doubts were raised[19,20] concerning the suitability of superhydrophobic coatings for long-term protection against electrochemical corrosion. The breakdown of the heterogeneous wetting regime of these coatings and the transition of wetting to the homogeneous regime was indicated as the main reason for a certain deterioration of anticorrosion ability during prolonged contact of a superhydrophobic surface with aggressive ions.

In this paper, we present a new approach to fabricating corrosion resistant coatings based on pulsed laser treatment followed by chemical surface modification. We will show the influence of the laser treatment parameters on the electrochemical behavior and wettability evolution of these superhydrophobic coatings in long-term contact with sodium chloride aqueous solutions. It will be demonstrated that intense laser treatment leading to the formation of a double layered structure of the coating containing an oxide sublayer with high

Received: July 10, 2015
Accepted: August 13, 2015
Published: August 13, 2015

DOI: 10.1021/acsami.5b06217
ACS Appl. Mater. Interfaces 2015, 7, 19500−19508

barrier properties and a textured sublayer with multimodal roughness makes it possible to fabricate a coating with a unique combination of properties, including water and ice repellency, corrosion resistance, and electrical insulation.

MATERIALS AND METHODS

Sample Preparation. In this paper, we fabricated and studied superhydrophobic coatings on the surface of AMG aluminum alloy (an analog of ISO AlMg3 alloy) with the following chemical composition (in weight %): Al 95.55, Mg 2.9, Mn 0.2, Cr 0.05, Cu 0.1, Fe 0.4, Si 0.4, Ti 0.1, Zn 0.2, and impurities 0.1. However, the procedure described here can easily be adapted to other aluminum alloys with the appropriate laser treatment parameters. The strategy for fabricating superhydrophobic surfaces is generally accepted now. It involves solving three problems.[21−26] First, it includes decreasing the surface energy of a material by treating the surface with hydrophobic agents. Second, increasing the local contact angle of a textured surface by choosing the appropriate shape of textural elements.[24] Finally, formation of a texture with multimodal roughness on the surface (by treating the surface layer of the material itself or by application of texturing elements made from other materials).

As discussed in recent reviews,[27−31] laser surface texturing has emerged as a novel and versatile nanotechnology for producing surfaces with multimodal roughness and high curvature of textural elements. Most studies in the literature have been conducted using femtosecond single-pulse duration laser treatment. At the same time, there has been increasing interest in nanosecond laser systems as a tool for surface processing in recent years.[32−36]

It is worth noting that laser surface texturing has an additional advantage compared to many other surface texturing methods. Namely, the interaction of high power radiation with condensed media may significantly affect the physicochemical properties of surface layers of the material, such as chemical and phase composition, microstructure, hardness, wear resistance, etc.[37,38]

In this study, we used an Argent-M laser system (Russia) with an IR ytterbium fiber laser (wavelength 1.064 μm), which provides a wide choice of laser parameters, and a RAYLASE MS10 2-axis laser beam deflection unit (Germany). Prior to laser treatment, the samples were degreased in a 1 M KOH solution, ultrasonically washed in deionized water and air-dried. Laser treatment was performed at ambient conditions with humidity of 40−50% and temperature of 20−25 °C.

Two different protocols were used for the surface laser treatment. For the first one, leading to fabrication of the superhydrophobic samples referred to in the following text as type 1 samples, we used one-fold laser treatment of the surface with pulse duration of 50 ns, repetition rate of 20 kHz, and peak power of 0.95 mJ in TEM_{00} mode. The samples were raster scanned at linear speed of 50 mm s^{-1} with parallel line density of 10 mm^{-1}. This treatment, accompanied by laser ablation and subsequent deposition of nanoparticles formed in the plasma onto the treated surface, leads to the formation of multimodal roughness on the aluminum alloy surface.

According to the second protocol, which we will refer to as intensive laser treatment, 10 repetitive runs, one after the other, with the same treatment parameters as described above, were applied to the sample surface, leading to increased duration of the high temperature state of the surface layers. The morphology of the type 2 samples obtained during intensive laser treatment is also characterized by multimodal roughness.

Both as-prepared surfaces just after the laser treatment are superhydrophilic, which is verified by rapid complete spreading of a water droplet along the surface.

The problem of surface energy reduction to transform the superhydrophilic state into the superhydrophobic one is easily solved today by using hydrocarbon or fluorocarbon surfactants.

However, as was shown in our recent paper,[39] the appropriate choice of surfactant is dictated by the application conditions of the sample. In this study, we have used fluorooxysilane, which is chemically adsorbed onto a textured surface and shows high chemical stability in brine, acidic and alkaline solutions.[39] Additional pretreatment of the laser textured surface was used before the chemisorption process to enrich the surface with hydroxyl groups serving as chemisorption centers. To do this, both types of samples were exposed to UV-ozone treatment (Bioforce Laboratories, USA) for 90 min. Immersion of the pretreated samples in a 1% solution of methoxy-{3-[(2,2,3,3,4,4,5,5,6,6,7,7,8,8,8-pentadecafluorooctyl)oxy]-propyl}-silane (hereinafter referred to as **MAF**) in decane for 2 h, followed by drying for 60 min in an oven at 130 °C results in the formation of a cross-linked layer of hydrophobic agent atop the laser textured surface with multimodal roughness.

The summary of the procedures used for sample preparation is presented in the Supporting Information (Table S1).

Measurement Techniques. The morphology of the sample surface and cross-section was studied using a Supra 40 VP (Carl Zeiss, Germany) field emission scanning electron microscope equipped with an INCA PentaFETx3 detector (Oxford Instruments, UK) for energy-dispersive X-ray spectroscopy (EDS). The SEM images were taken at 2−5 kV acceleration voltages and the Everhart-Thornley detector was used for the detection of the secondary electrons. All EDS spectra were obtained at 5 kV acceleration voltage.

The electrochemical properties of the fabricated coatings were studied using a PARSTAT 2273 potentiostat/galvanostat (Princeton Applied Research, USA). Measurements were carried out at room temperature in a three-electrode cell with a 0.5 M NaCl aqueous solution as an electrolyte. A silver/silver chloride electrode (Ag/AgCl) filled with saturated KCl solution served as a reference electrode, and a Pt mesh as a counter electrode. The corrosion medium was a 0.5 M solution of NaCl in contact with air maintained at 23 °C.

Deionized water with specific resistivity 18 MΩ cm and chemically pure grade reagents were used to prepare the electrolyte solutions. Prior to the electrochemical measurements, the samples were immersed in the solution for a certain time. The potentiodynamic polarization curves were registered at a scan rate of 1 mV/s in the applied potential range from-1.2 V to 0.6 V. A sinusoidal perturbation signal with amplitude of 20 mV (with respect to open circuit potential, OCP) was used for the electrochemical impedance spectroscopy (EIS) measurements. Impedance spectra were acquired in the frequency range from 0.05 Hz to 100 kHz with logarithmic sweep (20 points per decade). Corrosion potential, E_{corr}, and current, i_{corr}, were derived from the potentiodynamic polarization curves after Tafel extrapolation. After determining the Tafel constants from the anodic and cathodic slopes, the polarization resistance R_p was calculated according to the Stern-Geary method.[40]

Characterization of the wettability of the coatings was based on contact and rolling angle measurements. We used a homemade setup based on digital video image processing of sessile droplets to analyze the droplet shape parameters.[41,42] To characterize wetting of the coatings, we measured initial contact angles (CA) for 10−15 μL droplets at 10 different surface locations for each sample. For measurement of the rolling angle (RA), 10 μL droplets were deposited on the surface. After the initial droplet shape was equilibrated, manipulation with an angular positioner allowed us to change the sample surface tilt in a controllable manner and detect the rolling angle by averaging over 10 different droplets on the same substrate.

RESULTS AND DISCUSSION

The interaction of a high power laser beam with a material is accompanied by local heating, followed by rapid cooling of the surface layer, resulting in laser ablation, surface oxidation, grain refinement and collection of surface stresses. In addition, the nanoparticles formed in plasma due to laser-induced sublimation of surface layers are partially deposited on the treated surface.

The surface texture of a type 1 sample obtained by one-fold laser treatment of the surface is characterized by regular surface ripples and trenches with a period of 100 μm, decorated by fiber- and globule-like aggregates composed of nanoparticles (Figure 1). In addition to this regular ripple/trench micro-

DOI: 10.1021/acsami.5b06217
ACS Appl. Mater. Interfaces 2015, 7, 19500−19508

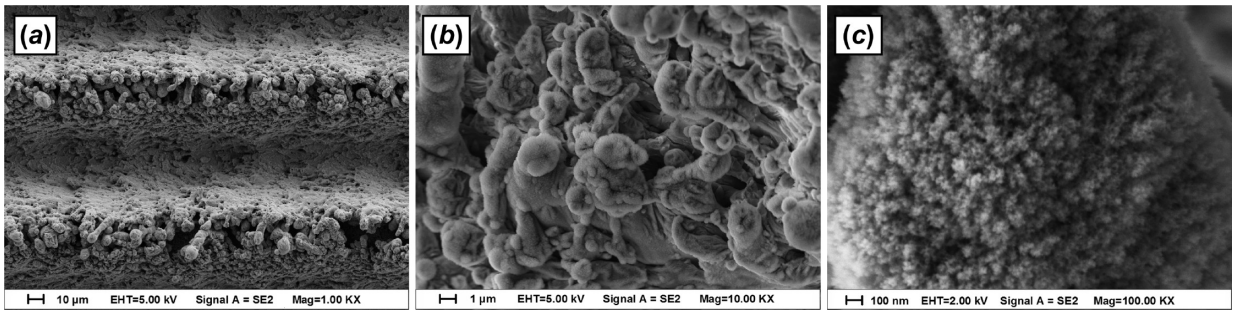

Figure 1. SEM images of the surface texture of a type 1 sample obtained by one-fold laser treatment at different length scales. Scale bars are (a) 10 μm, (b) 1 μm, and (c) 100 nm.

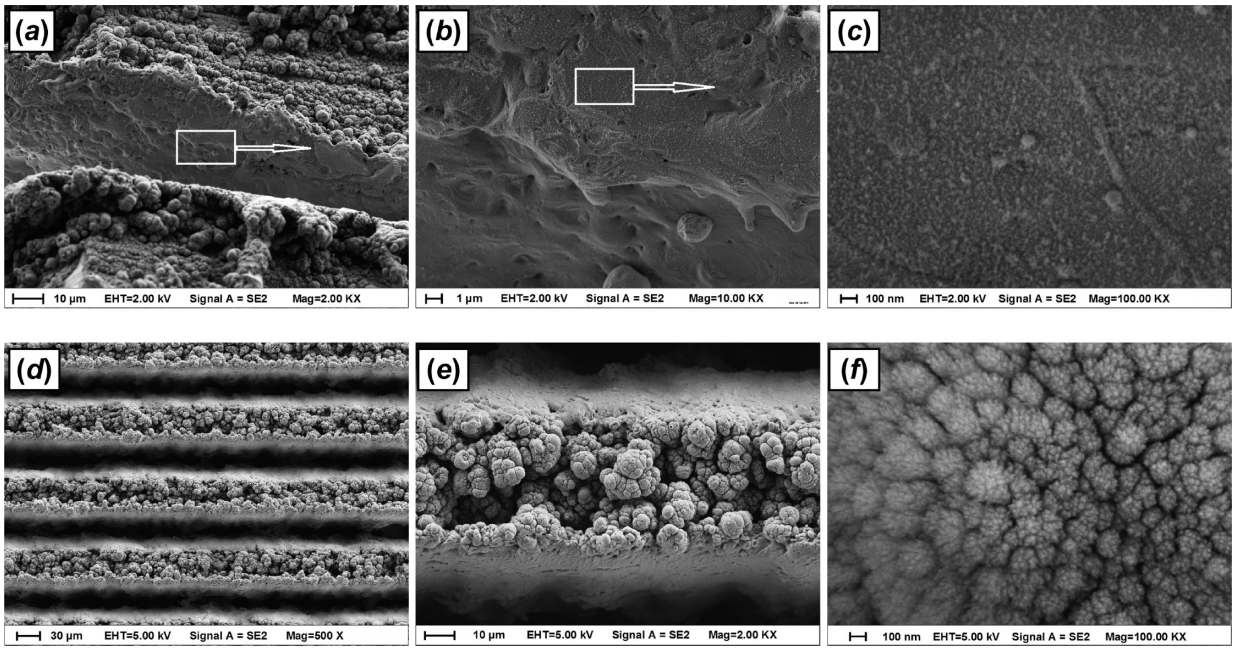

Figure 2. SEM images of the surface texture of the type 2 sample obtained by many-fold laser treatment at different length scales. (a–c) Side view, (d–f) top view. Scale bars are (a, e) 10 μm, (b) 1 μm, (c, f) 100 nm, and (d) 30 μm.

structure, two groups of characteristic sizes, namely the radii of aggregate curvature (on the order of 100–300 nm) and the size of the individual nanoparticles constituting the aggregates (varying from a few nanometers to tens of nanometers), are responsible for the multimodal roughness of the textured surface.

Many-fold intensive laser treatment makes it possible to maintain the melted state of surface layers in the presence of atmospheric oxygen much longer time than for type 1 samples, leading to the formation of a thicker oxide layer.[43]

At the same time, the high velocity of laser beam displacement results in rapid cooling of the surface layer, including the oxide skin layer. On the next laser pass during melting, the protective oxide skin is destroyed and is moved toward the inner layers by convection, whereas oxidation of the newly exposed top layer starts again. The metal undergoes multiple stages of melting and solidifying, resulting in excessive oxidation and the formation of a thick skin oxide layer covered by a layer of deposited nanoparticles. The detailed morphology of the type 2 sample is presented in Figure 2 and shows features of multimodal roughness similar to those of type 1 samples.

Chemical analysis of the nanoparticles deposited from a laser jet during laser ablation for the case of single-pulse nanosecond treatment in the presence of atmospheric oxygen[44] showed complete oxidation of aluminum to Al_2O_3. The EDS spectra obtained in our study for the top layers of the coating on both types of samples (marked by the rectangle *c* in Figure 3a, b) prior to their fluorination indicate a very high proportion of oxygen (see Figure 3c). The deviation of the ratio of O/Al content from the value characteristic of stoichiometric Al_2O_3 is apparently due to the fact that the EDS spectra collect information from the thick surface layer, including deposited nanoparticles, surface oxide and underlying aluminum alloy.

A comparison of EDS spectra for the regions d on the type 1 sample (Figure 3d) and region e on the type 2 sample (Figure 3e) shows that oxidation of the surface layer at a depth of about 100 μm below the bottom of the grooves is much higher for the type 2 sample (under intensive laser treatment) than for the type 1 sample.

In order to characterize the corrosion protective ability of samples associated with oxide skin layers formed during different laser treatment regimes, we compared the potentiodynamic polarization curves and impedance modulus spectra for three samples in a sodium chloride aqueous solution. The first and second samples were superhydrophilic and were obtained by one-fold and intensive laser treatment, respectively, as

DOI: 10.1021/acsami.5b06217
ACS Appl. Mater. Interfaces 2015, 7, 19500–19508

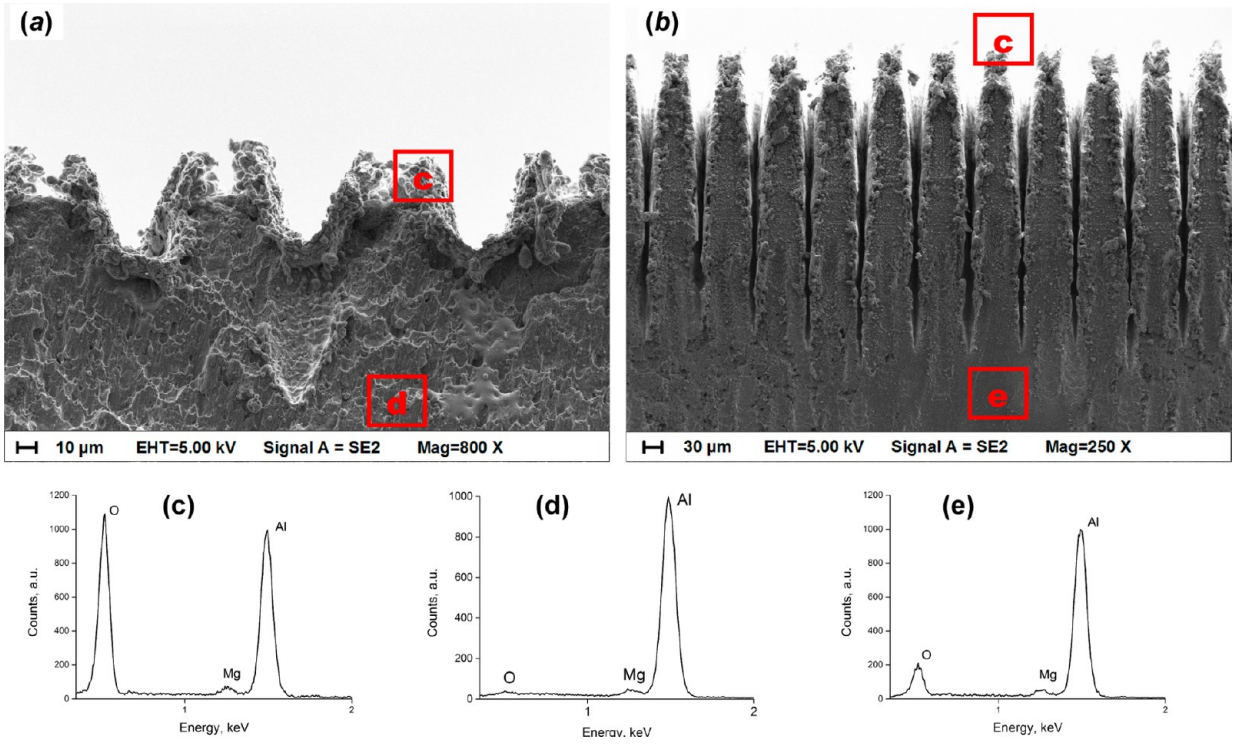

Figure 3. SEM cross-sectional views of (a) type 1 and (b) type 2 samples, and (c–e) EDS spectra typical of different regions of the cross-sections; corresponding regions are marked with bold rectangles on the SEM images. Scale bars are (a) 10 μm and (b) 30 μm.

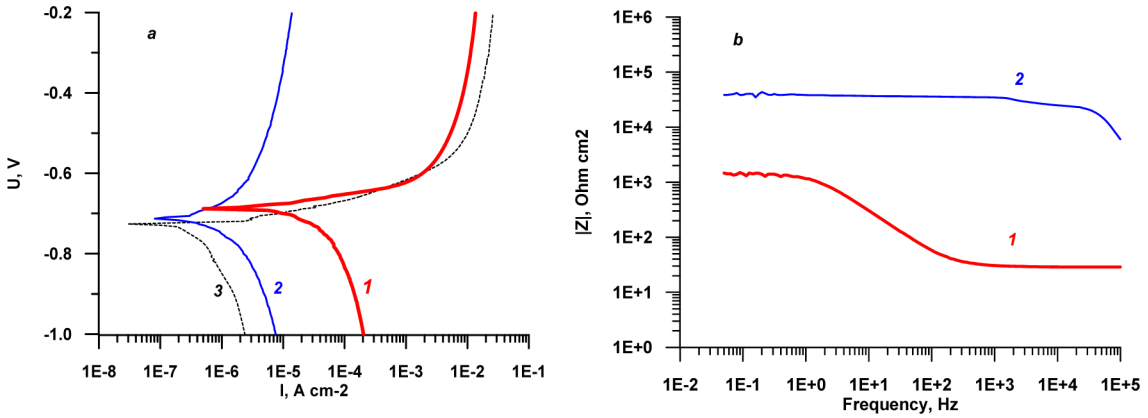

Figure 4. (a) Polarization curves for (1) one-fold and (2) many-fold laser-treated samples without hydrophobic treatment. (3) The polarization curve for an untreated sample with native oxide film is shown for comparison. The measurement of polarization curves for each sample began after 30 min of sample exposure to a 0.5 M NaCl solution. (b) Frequency dependence of the impedance modulus for (1) one-fold and (2) many-fold laser-treated samples after 30 min of sample exposure to a 0.5 M NaCl solution.

described above. Deposition of a hydrophobic agent was not used for these samples. We used a plate of the same AMG alloy with the native oxide layer ultrasonically washed in ethanol for 5 min as the third sample. The data presented in Figure 4a show that in brine solution, the native oxide film on aluminum–magnesium alloy (sample 3) has low solubility, and a small current is measured at open circuit potential.

Laser texturing leads to the activation of cathodic reactions associated for both textured samples with the reduction of oxygen dissolved in brine solution, due to the presence of defects in the oxide film and an increase in the actual sample/solution contact area associated with surface roughening during laser treatment. At the same time, the anodic reaction for sample 2 is essentially passivated, indicating high barrier properties of the thick oxide layer formed on top of the alloy surface due to intense laser treatment. The behavior of the impedance modulus for the laser-treated samples (Figure 4b) gives clear evidence of much better barrier properties of the oxide layer formed on an aluminum–magnesium alloy surface under intense laser treatment compared to one-fold treatment.

The results for corrosion resistance obtained here are in line with the literature data. It is known that an increase in both the thickness of the dense oxide layer and the time of oxidation enhances anticorrosion performance.[43,45] The porosity and structure of oxide obtained by thermal oxidation of Al are strongly dependent on the temperature of oxidation as well.[8,46,47] It was shown in the literature that the oxide layer consists of a composite type of Al_2O_3, $Al(OH)_3$, and $AlO(OH)$. Variation in the oxide layer composition results in a change in chemical reactivity of the oxide with the chloride ion and its

DOI: 10.1021/acsami.5b06217
ACS Appl. Mater. Interfaces 2015, 7, 19500–19508

Table 1. Typical Contact and Rolling Angles for Different Superhydrophobic Coatings

state of the coating	superhydrophobic sample type 1, one-fold laser treatment		superhydrophobic sample type 2, intensive laser treatment	
	CA (deg)	RA (deg)	CA (deg)	RA (deg)
freshly prepared coatings	173.1 ± 1.2	2.1 ± 0.6	173.4 ± 1.0	2.4 ± 1.2
after measurement of the polarization curve for samples immersed in a 0.5 M NaCl solution for 240 h	167.2 ± 0.8	7.4 ± 2.9	168.6 ± 2.7	10.4 ± 4.4

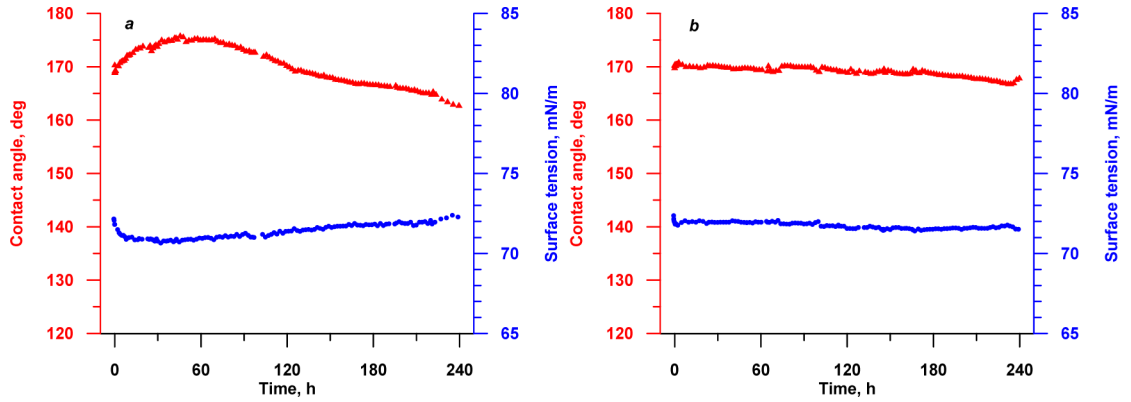

Figure 5. Long-term evolution of contact angle (red triangles) and surface tension (blue circles) of a droplet of 0.5 M NaCl aqueous solution on the surface of superhydrophobic samples of (a) type 1 and (b) type 2.

porosity, and thereafter corrosion resistance.[8,47] The results presented in ref 8 suggest that transformation of the surface oxide film into the AlO(OH) phase enhances the passivity of the Al surface, and thereafter corrosion resistance in a chloride solution. The porosity of above oxide film was not stated explicitly; however, from the given values of both ionic and electronic charge transfer resistance, it is assumed that the porosity was low. In contrast, studies of the electrochemical behavior of protective aluminum oxide coatings deposited by the metal−organic CVD method at various temperatures[47] have shown that amorphous AlO(OH) coatings deposited at 623 K had limited corrosion protection because of their lamellar nanostructure. Amorphous, porosity-free Al_2O_3 deposited above 688 K showed improvement of corrosion resistance by 2 orders of magnitude compared to the bare alloy.

In our study, the oxide layer for sample 2 was formed during longer exposure at temperatures above the melting point than for sample 1. High temperature oxidation was also accompanied by multiple stages of melting and solidifying with convective displacement of the broken oxide layer into deeper layers, followed by further oxidation of the top layer. The combination of these processes leads to the formation of a thick skin oxide layer with very low porosity (Figure 2b, d), under the layer of deposited Al_2O_3 nanoparticles.

Now let us consider how the superhydrophobic state of samples achieved after chemisorption of fluorooxysilanes onto the laser textured surface will influence the protective properties of the fabricated coatings. Typical contact and rolling angles measured for both freshly prepared superhydrophobic coatings are presented in Table 1.

The chemical binding of hydrophobic agent to laser textured surfaces of both types was validated using FT-IR spectroscopy by comparison of absorbance spectra of textured samples with and without deposited hydrophobic agent and of MAF layer deposited onto KBr optical window. The measured spectra and their discussion are presented in the Supporting Information.

Although the thickness and structure of the oxide layer, as well as the surface morphologies of the two samples, differ from each other (compare Figures 1 and 2), the wettability parameters are close to each other. The similarity of the values of contact and rolling angles indicates that initial wettability is mainly determined by the top layer of deposited Al_2O_3 nanoparticles, with chemisorbed MAF. Thus, the morphology and chemistry of the wetted parts are the same for both samples (Figures 1c and 2f). In order to analyze the interaction of type 1 and type 2 samples with brine solution, we studied the long-term evolution of contact angle and surface tension of a droplet of 0.5 M NaCl aqueous solution over 240 h. To eliminate droplet evaporation, we exposed the superhydrophobic samples with a droplet to a saturated water vapor atmosphere, as described in ref 48. As shown in the literature,[48] the chemical instability of a superhydrophobic coating contacting with an aqueous medium results in deterioration of the contact angle and a sharp decrease in droplet surface tension due to desorption of the hydrophobic agent from the coating/liquid interface with formation of a terminal silanol group, and transfer to the liquid/vapor interface. In contrast, stability is revealed by the constant values of both contact angle and surface tension.

The data presented in Figure 5b, indicate that both considered parameters of an aqueous droplet in contact with the sample remain nearly constant over 10 days, leading to the conclusion that the sample fabricated by intense laser treatment and chemisorption of MAF has very high chemical stability in sodium chloride solutions. The rolling angle for the droplet analyzed in the experiment was 2.1° after 10 days of contact between droplet and coating. The situation is a bit different (Figure 5a) for the type 1 sample. Weak growth of the contact angle accompanying the decrease in droplet surface tension σ_{lv} is detectable during 60 h of contact between the droplet and sample. The physical reason for this decrease in σ_{lv} is the partial removal of molecules of the hydrophobic agent from the coating/liquid interface due to its interaction with the sodium

DOI: 10.1021/acsami.5b06217
ACS Appl. Mater. Interfaces 2015, 7, 19500−19508

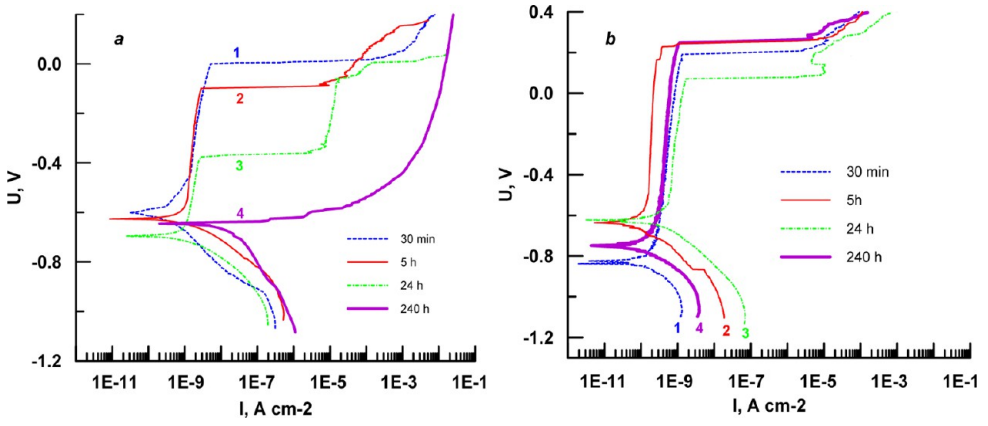

Figure 6. Potentiodynamic polarization curves for superhydrophobic samples of (a) type 1 and (b) type 2 measured after different exposure times of the sample to a 0.5 M NaCl aqueous solution: (1) 30 min, (2 5 h), (3) 24 h, and (4) 240 h.

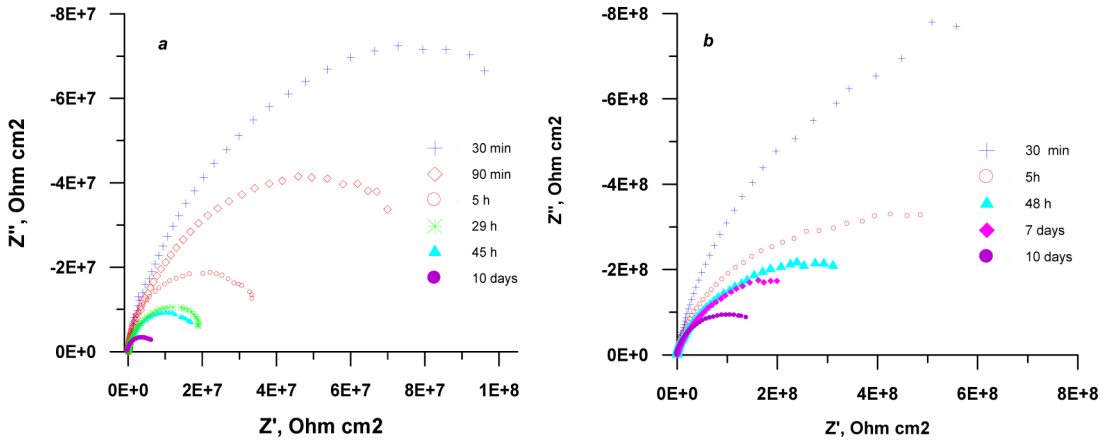

Figure 7. Nyquist plots for superhydrophobic samples of (a) type 1 and (b) type 2 measured after different exposure times (indicated in the legend) of the sample to a 0.5 M NaCl aqueous solution.

chloride solution and redistribution between the bulk of the droplet and droplet/air interface. Such decrease in σ_{lv}, at nearly constant wetting tension ($\sigma_{sv}-\sigma_{sl}$) for hydrophobic materials results (according to Young equation) in increase in the value of Young contact angle at local three phase equilibrium. Therefore, the measured contact angle for the coatings (according to Cassie–Baxter equation) is increased concomitantly with surface tension decrease. As a result, the formation of wetting defects at the coating/droplet interface and the presence of aggressive ions like chloride causes a mass transfer of components of the solution through the coating, extensive localized attack and the corrosion processes of aluminum.[49] The dissolution of aluminum leads to an increase in the solution/substrate contact area, which in turn causes the transition of MAF molecules from the droplet/air interface toward the freshly formed interface and their readsorption in order to decrease the total Gibbs energy of the system. The combination of the above-mentioned processes is revealed as an increase in droplet surface tension and weak deterioration of the contact angle at large time scales of contact between the droplet and coating (Figure 5a). Thus, the results of the 10-day wetting experiment lead to the conclusion that the type 1 sample is subjected to corrosion processes. The potentiodynamic polarization curves (Figure 6) and EIS data (Figure 7) as a function of exposure time were used to study the corrosion protective properties of both samples during long-term contact with brine solution in more detail. The corrosion potential E_{corr}, corrosion current i_{corr}, and polarization resistance (R_p) presented in Table 2 were calculated from the polarization curves.

Table 2. Electrochemical Parameters of the Samples

sample, time of exposure in brine solution	E_{corr} (V)	i_{corr}(A/cm^2)	R_p (Ω cm^2)
nontextured AMG alloy with native oxide, 30 min	−0.730	1.0×10^{-6}	6.8×10^{4}
sample type 1, 30 min	−0.601	2.3×10^{-10}	4.2×10^{8}
sample type 1, 5 h	−0.610	1.0×10^{-9}	2.2×10^{7}
sample type 1, 24 h	−0.700	1.0×10^{-9}	1.9×10^{7}
sample type 1, 240 h	−0.651	2.0×10^{-8}	1.4×10^{5}
sample type 2, 30 min	−0.830	1.8×10^{-10}	2.5×10^{8}
sample type 2, 5 h	−0.637	1.3×10^{-10}	2.9×10^{8}
sample type 2, 24 h	−0.623	5.0×10^{-10}	1.3×10^{8}
sample type 2, 120 h	−0.559	4.2×10^{-10}	1.0×10^{8}
sample type 2, 240 h	−0.750	3.0×10^{-10}	2.4×10^{8}

Consistent with the results of the wetting experiments, analysis of the electrochemical data indicates that the type 2 sample demonstrates better protective performance against corrosion on long-term contact with a chloride-containing electrolyte. The polarization resistance, R_p, which is commonly used as a measure of the resistance of a metal to corrosion damage, had a value of 2.4×10^8 Ω cm^2 after 240 h of sample

DOI: 10.1021/acsami.5b06217
ACS Appl. Mater. Interfaces 2015, 7, 19500−19508

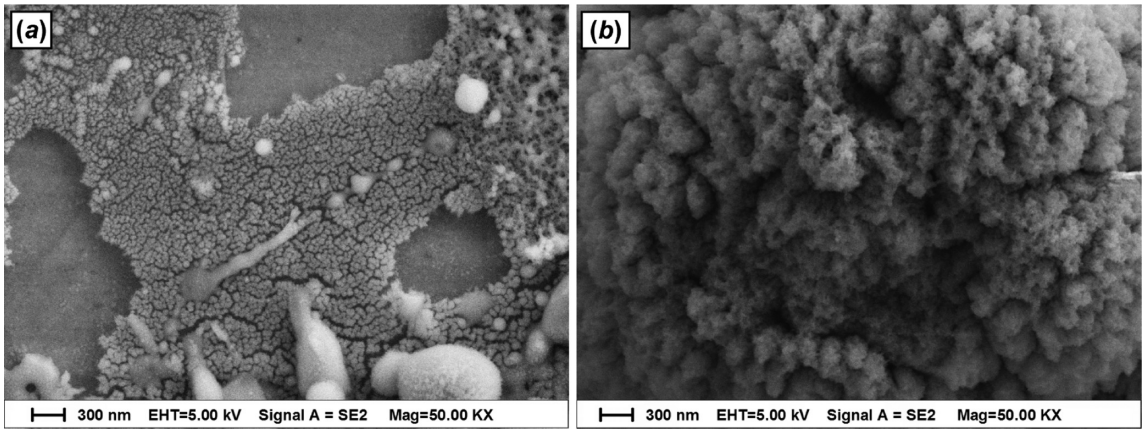

Figure 8. SEM images of the surface of superhydrophobic samples of (a) type 1 and (b) type 2 after 10 days of exposure of the sample to a 0.5 M NaCl aqueous solution followed by a measurement of polarization curves. Scale bars are 300 nm for both images.

immersion in the solution. This value of R_p, indicating high stability during the time of contact with the solution, is associated with high corrosion prevention capability.[50] The difference between corrosion currents for this sample and the nontextured AMG alloy with native oxide is up to 4 orders of magnitude (Table 2).

In contrast, the initial polarization resistance of the sample, which is 4 orders of magnitude higher than for the reference sample with native oxide and even higher than the initial resistance of the type 2 sample, deteriorates to $1.4 \times 10^5\ \Omega\ cm^2$ over 10 days of immersion in the solution.

The polarization curves for the type 1 sample show essential passivation of the anodic reaction for short immersion times. As a result, the pitting potential E_{pit} shifts toward positive values. As was discussed in ref 49, localized corrosion can be prevented by chemisorbed organic molecules, which preclude the adsorption of aggressive anions, or by the formation of a more resistant oxide film on the metal surface, while the difference $E_{pit} - E_{corr}$ is able to account for the efficiency of inhibiting localized corrosion.

The significant decrease in the cathodic current (compare Figures 6a and 4a) compared to the reference sample shows that oxygen reduction is also limited in the presence of a superhydrophobic layer. However, as immersion time increases, deterioration of the protective properties of the coating causes the pitting potential to approach the corrosion potential; and after 10 days, the passive state of the anodic branch is no longer detected, while the cathodic branch of the polarization curve approaches that of the sample with native oxide. The partial corrosive damage of superhydrophobic sample type 1 in a sodium chloride solution after a few days of immersion is also revealed by the temporal evolution of Nyquist diagrams (Figure 7a), although the impedance modulus for low frequencies still remains higher than $1 \times 10^6\ \Omega\ cm^2$. Behavior during immersion is different for the type 2 sample. After 10 days, the plateau in the anodic branch indicating passivation of the anodic reaction is still characterized by a large value of $E_{pit} - E_{corr}$, with a positive value of pitting potential, and cathodic current is still essentially lower than for the reference sample. At the same time, weak deterioration of the coating as the immersion time increases is revealed by some growth in the cathodic current and shrinking of Nyquist diagrams, while preserving capacitive response.

Because polarization of the coatings during polarization curve measurement may cause loss of the superhydrophobic state due to the electrowetting effect, we measured the contact and rolling angles for samples immersed in the solution for 240 h and then subjected to polarization curve measurement. The results of these measurements presented in Table 1, together with visual testing of the sample surfaces, convince us that that the superhydrophobic state for both samples is quite resistant to electrowetting caused by polarization of the sample surface.

Thus, the corrosion damage occurring on the type 1 sample during 10 days of immersion is of a local nature and is associated with the formation of micropits. Such micropits were detected by the electron microscopy study of the samples, used for measurement of polarization curves after 10 days of immersion (Figure 8). The presence of micropits is easily seen on the surface of type 1 sample. In contrast, for the type 2 sample only moderate distortion of the spatial homogeneity of nanoparticles distribution along the surface is detected.

CONCLUSIONS

Nanosecond laser treatment followed by surface modification with low surface energy fluorooxysilanes was used in this study to fabricate superhydrophobic coatings on AMG aluminum−magnesium alloy. We have shown that one of the most important steps in fabricating superhydrophobic coatings, i.e., surface texturing applied to impart multimodal roughness, may be simultaneously used for modifying the physicochemical properties of the thick surface layer of the substrate itself. Coatings with different barrier properties of the oxide layer were fabricated by varying the laser treatment parameters. We have found that during intensive laser treatment, the interaction of a high power nanosecond laser beam with an aluminum alloy is accompanied by very local heating and rapid cooling of the surface layer, resulting in the formation of an oxide surface layer with good barrier properties for transfer of charges, chloride ions and water molecules. Subsequent chemisorption of the hydrophobic agent onto the laser treated surface makes it possible to achieve the superhydrophobic state of an aluminum alloy surface.

Analysis of the evolution of wetting and electrochemical properties for different superhydrophobic samples immersed in a sodium chloride solution was performed to estimate the corrosion resistance of the coatings. It was demonstrated that the superhydrophobic state of a metal surface inhibits the corrosion processes in chloride solutions due to the presence of a protective layer of air trapped inside the grooves of the surface

DOI: 10.1021/acsami.5b06217
ACS Appl. Mater. Interfaces 2015, 7, 19500−19508

texture and separating the alloy surface from the aggressive liquid medium. Another important protective factor for these coatings is related to the formation of a cross-linked chemisorbed monolayer of hydrophobic agent. However, during long-term contact of a superhydrophobic coating with a solution, the wetted area of the coating is subjected to corrosion processes due to the formation of defects. Thus, when water repellence of the surface is the only mechanism used to protect against corrosion, these superhydrophobic coatings cannot be used as durable protection for surfaces continuously immersed in electrolytes. However, remarkable resistance is characteristic of the superhydrophobic coatings obtained by intense laser treatment, followed by chemisorption of the hydrophobic agent. Electrochemical and wetting experiments showed that the protective potential is significantly enhanced. We attribute this to the synergetic effect between the protective properties of air trapped in a rough superhydrophobic surface, barrier properties of the chemisorbed layer of fluorooxysilane that suppress chloride ion adsorption, and good barrier properties of the thick oxide sublayer with low porosity that retard the transfer of charges, chloride ions, and water molecules.

■ ASSOCIATED CONTENT

Supporting Information

The Supporting Information is available free of charge on the ACS Publications website at DOI: 10.1021/acsami.5b06217.

Brief summary of the procedures used for sample preparation (Table S1) and FT-IR spectroscopic data (Figure S1) proving the chemical binding of hydrophobic agent to laser textured surfaces (PDF)

■ AUTHOR INFORMATION

Corresponding Author

*E-mail: boinovich@mail.ru.

Notes

The authors declare no competing financial interest.

■ ACKNOWLEDGMENTS

The work was supported by the Russian Science Foundation (Grant 14-13-01076).

■ REFERENCES

(1) Ambat, R.; Davenport, A.; Scamans, M.; Afseth, A. Effect of Iron-Containing Intermetallic Particles on the Corrosion Behaviour of Aluminium. *Corros. Sci.* **2006**, *48*, 3455−3471.

(2) Rodriguez-Diaz, R. A.; Uruchurtu-Chavarin, J.; Cotero-Villegas, A. M.; Valdez, S.; Juárez-Islas, J. A. Corrosion Behavior of AlMgSi Alloy in Aqueous Saline Solution. *Int. J. Electrochem. Sci.* **2015**, *10*, 1792−1808.

(3) Figueira, R. B.; Silva, C. J. R.; Pereira, E. V. Organic−Inorganic Hybrid Sol−Gel Coatings for Metal Corrosion Protection: A Review of Recent Progress. *J. Coat. Technol. Res.* **2015**, *12*, 1−35.

(4) Sorensen, P. A.; Kiil, S.; Dam-Johansen, K.; Weinell, C. E. Anticorrosive Coatings: A Review. *J. Coat. Technol. Res.* **2009**, *6*, 135−176.

(5) Duran, A.; Castro, Y.; Aparicio, M.; Conde, A.; de Damborenea, J. J. Protection and Surface Modification of Metals with Sol−Gel Coatings. *Int. Mater. Rev.* **2007**, *52*, 175−192.

(6) Balaskas, A. C.; Kartsonakis, I. A.; Snihirova, D.; Montemor, M. F.; Kordas, G. Improving the Corrosion Protection Properties of Organically Modified Silicate−Epoxy Coatings by Incorporation of Organic and Inorganic Inhibitors. *Prog. Org. Coat.* **2011**, *72*, 653−662.

(7) Garrigues, L.; Pebere, N.; Dabosi, F. An Investigation of the Corrosion Inhibition of Pure Aluminum in Neutral and Acidic Chloride Solutions. *Electrochim. Acta* **1996**, *41*, 1209−1215.

(8) Lee, E. J.; Pyun, S. I. The Effect of Oxide Chemistry on the Passivity of Aluminium Surfaces. *Corros. Sci.* **1995**, *37*, 157−168.

(9) Lu, Z.; Wang, P.; Zhang, D. Super-Hydrophobic Film Fabricated on Aluminium Surface as a Barrier to Atmospheric Corrosion in a Marine Environment. *Corros. Sci.* **2015**, *91*, 287−296.

(10) Cheng, Y.; Lu, S.; Xu, W.; Wen, H. Fabrication of Au−$AlAu_4$−Al_2O_3 Superhydrophobic Surface and its Corrosion Resistance. *RSC Adv.* **2015**, *5*, 15387−15394.

(11) Ou, J.; Liu, M.; Li, W.; Wang, F.; Xue, M.; Li, C. Corrosion Behavior of Superhydrophobic Surfaces of Ti Alloys in NaCl Solutions. *Appl. Surf. Sci.* **2012**, *258*, 4724−4728.

(12) Boinovich, L. B.; Gnedenkov, S. V.; Alpysbaeva, D. A.; Egorkin, V. S.; Emelyanenko, A. M.; Sinebryukhov, S. L.; Zaretskaya, A. K. Corrosion Resistance of Composite Coatings on Low-Carbon Steel Containing Hydrophobic and Superhydrophobic Layers in Combination with Oxide Sublayers. *Corros. Sci.* **2012**, *55*, 238−245.

(13) Ejenstam, L.; Ovaskainen, L.; Rodriguez-Meizoso, I.; Wagberg, L.; Pan, J. S.; Swerin, A.; Claesson, P. M. The Effect of Superhydrophobic Wetting State on Corrosion Protection - the AKD Example. *J. Colloid Interface Sci.* **2013**, *412*, 56−64.

(14) Lv, D.; Ou, J.; Xue, M.; Wang, F. Stability and Corrosion Resistance of Superhydrophobic Surface on Oxidized Aluminum in NaCl Aqueous Solution. *Appl. Surf. Sci.* **2015**, *333*, 163−169.

(15) Liang, J.; Hu, Y.; Wu, Y.; Chen, H. Facile Formation of Superhydrophobic Silica-Based Surface on Aluminum Substrate with Tetraethylorthosilicate and Vinyltriethoxysilane as Co-Precursor and its Corrosion Resistant Performance in Corrosive NaCl Aqueous Solution. *Surf. Coat. Technol.* **2014**, *240*, 145−153.

(16) Khorsand, S.; Raeissi, K.; Ashrafizadeh, F. Corrosion Resistance and Long-Term Durability of Super-Hydrophobic Nickel Film Prepared by Electrodeposition Process. *Appl. Surf. Sci.* **2014**, *305*, 498−505.

(17) Boinovich, L. B.; Emelyanenko, A. M.; Pashinin, A. S.; Gnedenkov, S. V.; Egorkin, V. S.; Sinebryukhov, S. L. Mg Alloy Treatment for Superhydrophobic Anticorrosion Coatings Formation. *Surf. Innovations* **2013**, *1*, 157−167.

(18) Ejenstam, L.; Swerin, A.; Pan, J. S.; Claesson, P. M. Corrosion Protection by Hydrophobic Silica Particle-Polydimethylsiloxane Composite Coatings. *Corros. Sci.* **2015**, DOI: 10.1016/j.corsci.2015.06.018.

(19) Yu, D. Y.; Tian, J. T. Superhydrophobicity: Is it Really Better than Hydrophobicity on Anti-Corrosion? *Colloids Surf., A* **2014**, *445*, 75−78.

(20) Qiu, R.; Zhang, D.; Wang, P. Superhydrophobic-Carbon Fibre Growth on a Zinc Surface for Corrosion Inhibition. *Corros. Sci.* **2013**, *66*, 350−359.

(21) Boinovich, L. B.; Emelyanenko, A. M. Hydrophobic Materials and Coatings: Principles of Design, Properties and Applications. *Russ. Chem. Rev.* **2008**, *77*, 619−638.

(22) Boinovich, L.; Emelyanenko, A. Principles of Design of Superhydrophobic Coatings by Deposition from Dispersions. *Langmuir* **2009**, *25*, 2907−2912.

(23) Xia, F.; Jiang, L. Bio-Inspired, Smart, Multiscale Interfacial Materials. *Adv. Mater.* **2008**, *20*, 2842−2858.

(24) Boinovich, L.; Emelyanenko, A. The Prediction of Wettability of Curved Surfaces on the Basis of the Isotherms of the Disjoining Pressure. *Colloids Surf., A* **2011**, *383*, 10−16.

(25) Quere, D. Non-Sticking Drops. *Rep. Prog. Phys.* **2005**, *68*, 2495−2532.

(26) Nosonovsky, M.; Bhushan, B. Superhydrophobic Surfaces and Emerging Applications: Non-Adhesion, Energy, Green Engineering. *Curr. Opin. Colloid Interface Sci.* **2009**, *14*, 270−280.

(27) Stratakis, E. Nanomaterials by Ultrafast Laser Processing of Surfaces. *Sci. Adv. Mater.* **2012**, *4*, 407−431.

DOI: 10.1021/acsami.5b06217
ACS Appl. Mater. Interfaces 2015, 7, 19500−19508

(28) Chen, F.; Zhang, D.; Yang, Q.; Yong, J.; Du, G.; Si, J.; Yun, F.; Hou, X. Bioinspired Wetting Surface via Laser Microfabrication. *ACS Appl. Mater. Interfaces* **2013**, *5*, 6777−6792.
(29) Sugioka, K.; Cheng, Y. Ultrafast Lasers − Reliable Tools for Advanced Materials Processing. *Light: Sci. Appl.* **2014**, *3*, e149.
(30) Vorobyev, A. Y.; Guo, C. Femtosecond Laser Modification of Material Wetting Properties: A Brief Review. *Sci. Adv. Mater.* **2012**, *4*, 432−438.
(31) Boinovich, L. B.; Domantovskiy, A. G.; Emelyanenko, A. M.; Pashinin, A. S.; Ionin, A. A.; Kudryashov, S. I.; Saltuganov, P. N. Femtosecond Laser Treatment for the Design of Electro-Insulating Superhydrophobic Coatings with Enhanced Wear Resistance on Glass. *ACS Appl. Mater. Interfaces* **2014**, *6*, 2080−2085.
(32) Li, B. J.; Zhou, M.; Zhang, W.; Amoako, G.; Gao, C. Y. Comparison of Structures and Hydrophobicity of Femtosecond and Nanosecond Laser-Etched Surfaces on Silicon. *Appl. Surf. Sci.* **2012**, *263*, 45−49.
(33) Pazokian, H.; Selimis, A.; Barzin, J.; Jelvani, S.; Mollabashi, M.; Fotakis, C.; Stratakis, E. Tailoring the Wetting Properties of Polymers from Highly Hydrophilic to Superhydrophobic Using UV Laser Pulses. *J. Micromech. Microeng.* **2012**, *22*, 035001.
(34) Psarski, M.; Marczak, J.; Grobelny, J.; Celichowski, G. Superhydrophobic Surface by Replication of Laser Micromachined Pattern in Epoxy/Alumina Nanoparticle Composite. *J. Nanomater.* **2014**, *2014*, 547895.
(35) Emelyanenko, A. M.; Shagieva, F. M.; Domantovsky, A. G.; Boinovich, L. B. Nanosecond Laser Micro- and Nanotexturing for the Design of a Superhydrophobic Coating Robust against Long-Term Contact with Water, Cavitation, and Abrasion. *Appl. Surf. Sci.* **2015**, *332*, 513−517.
(36) Boinovich, L. B.; Emelyanenko, A. M.; Emelyanenko, K. A. Effect of Decanol Vapors on the Delay in Water Droplet Crystallization on Superhydrophobic Substrates. *J. Phys. Chem. C* **2015**, *119*, 8718−8724.
(37) Kusinski, J.; Kac, S.; Kopia, A.; Radziszewska, A.; Rozmus-Górnikowska, M.; Major, B.; Major, L.; Marczak, J.; Lisiecki, A. Laser Modification of the Materials Surface Layer − A Review Paper. *Bull. Pol. Acad. Sci.: Tech. Sci.* **2012**, *60*, 711−728.
(38) Kharanzhevskiy, E. V.; Krivilyov, M. D.; Reshetnikov, S. M.; Sadiokov, E. E.; Gil'mutdinov, F. Z. Corrosion-Electrochemical Behavior of Nanostructured Chromium Oxide Layers Obtained by Laser Irradiation of Unalloyed Steel by Short Pulses. *Prot. Met. Phys. Chem. Surf.* **2014**, *50*, 777−783.
(39) Boinovich, L. B.; Emelyanenko, A. M. The Behaviour of Fluoro- and Hydrocarbon Surfactants Used for Fabrication of Superhydrophobic Coatings at Solid/Water Interface. *Colloids Surf., A* **2015**, *481*, 167−175.
(40) Stern, M.; Geary, A. L. Electrochemical Polarization I. A Theoretical Analysis of the Shape of Polarization Curves. *J. Electrochem. Soc.* **1957**, *104*, 56−63.
(41) Emel'yanenko, A. M.; Boinovich, L. B. The Use of Digital Processing of Video Images for Determining Parameters of Sessile and Pendant Droplets. *Colloid J.* **2001**, *63*, 159−172.
(42) Emelyanenko, A. M.; Boinovich, L. B. The Role of Discretization in Video Image Processing of Sessile and Pendant Drop Profiles. *Colloids Surf., A* **2001**, *189*, 197−202.
(43) Schmitz, Ch. *Handbook of Aluminium Recycling*; Vulkan Verlag: Essen, Germany, 2006.
(44) Libenson, M. N.; Shandybina, G. D.; Shakhmin, A. L. Chemical Analysis of Products Obtained by Nanosecond Laser Ablation. *Tech. Phys.* **2000**, *45*, 1219−1222.
(45) Guidi, F.; Moretti, G.; Carta, G.; Natali, M.; Rossetto, G.; Pierino, Z.; Salmaso, G.; Rigato, V. Electrochemical Anticorrosion Performance Evaluation of Al_2O_3 Coatings Deposited by MOCVD on an Industrial Brass Substrate. *Electrochim. Acta* **2005**, *50*, 4609−4614.
(46) Gleizes, A. N.; Vahlas, C.; Sovar, M. M.; Samélor, D.; Lafont, M. C. CVD-Fabricated Aluminum Oxide Coatings from Aluminum Tri-Iso-Propoxide: Correlation between Processing Conditions and Composition. *Chem. Vap. Deposition* **2007**, *13*, 23−29.
(47) Boisier, G.; Raciulete, M.; Samélor, D.; Pébère, N.; Gleizes, A. N.; Vahlas, C. Electrochemical Behavior of Chemical Vapor Deposited Protective Aluminum Oxide Coatings on Ti6242 Titanium Alloy. *Electrochem. Solid-State Lett.* **2008**, *11* (10), C55−C57.
(48) Boinovich, L. B.; Emelyanenko, A. M. A Wetting Experiment as a Tool to Study the Physicochemical Processes Accompanying the Contact of Hydrophobic and Superhydrophobic Materials with Aqueous Media. *Adv. Colloid Interface Sci.* **2012**, *179*, 133−141.
(49) Szklarska-Smialowska, Z. Pitting Corrosion of Aluminum. *Corros. Sci.* **1999**, *41*, 1743−1767.
(50) Leidheiser, H. Electrical and Electrochemical Measurements as Predictors of Corrosion at the Metal-Organic Coating Interface. *Prog. Org. Coat.* **1979**, *7*, 79−104.

DOI: 10.1021/acsami.5b06217
ACS Appl. Mater. Interfaces 2015, 7, 19500−19508